Liu, Z.; Feyerabend, F.; Bohlen, J.; Willumeit-Roemer, R.; Letzig, D.:
Mechanical properties and degradation behavior of binary magnesium-silver alloy sheets.
In: Journal of Physics and Chemistry of Solids. Vol. 133 (2019) 142 - 150.
First published online by Elsevier: 17.05.2019

https://dx.doi.org/10.1016/j.jpcs.2019.05.008

Mechanical properties and degradation behavior of binary magnesium-silver alloy sheets

Zhidan Liu [1,2], Frank Feyerabend [1]*, Jan Bohlen [3], Regine Willumeit-Römer [1], Dietmar Letzig [3]

* Corresponding author: Dr. Frank Feyerabend, Phone: +49 (0)4152 871259, Fax: +49 (0)4152 872595, E-mail: frank.feyerabend@hzg.de

1. Metallic Biomaterials, Institute of Materials Research, Helmholtz-Zentrum Geesthacht, Max-Planck-Str. 1, 21502 Geesthacht, Germany

2. National Engineering Research Center for Healthcare Devices, Guangdong Institute of Medical Instruments, Guangzhou Guangdong 510500, China

3. Magnesium Innovation Center, Institute of Materials Research, Helmholtz-Zentrum Geesthacht, Max-Planck-Str. 1, 21502 Geesthacht, Germany

Abstract

The application of Mg-Ag alloys is suggested as biodegradable implant materials in the form of sheets with controllable mechanical properties and appropriate degradation behavior. This study aimed on the understanding of influence of rolling temperature and silver content (2 -8 wt %) on the microstructure development, mechanical properties and the degradation behavior of the sheet material. Besides an increase of the average grain size with increasing rolling temperature, precipitates of $Mg_{54}Ag_{17}$ formed during processing at lower temperatures and resulted in grain growth restriction during recrystallization. A typical alignment of basal planes parallel to the sheet plane was confirmed by texture measurements along with a strengthening of such textures when grains grew larger during recrystallization. As a result, an increase of the Ag-content corresponds to an increase in the hardness and strength properties of the sheets. In immersion tests, the as-rolled and annealed Q6 and Q8 rolled at 400 °C or 450 °C had similar degradation rate but an obvious difference of the degradation morphology

due to the existence of precipitates at grain boundaries. By elevating the rolling and annealing temperature, the degradation rate decreased and the elimination of precipitates led to homogeneous degradation even when the silver in magnesium was up to 8 wt.%. Appropriate short time annealing procedures below 60 s allow the tailored regulation of hardness, mechanical properties and ductility via controlled static recrystallization.

Keywords: rolling, (short time) annealing, microstructure, texture, mechanical properties, degradation behavior

Highlights:

- Thermo-mechanical treatment of Mg-Ag alloys leads to coarse grains by enhanced recrystallization and grain growth
- Adjusted short time annealing allows tailored grain structure development with impact on the mechanical properties
- A solid solution strengthening effect of Ag is maintained during rolling and annealing
- Precipitation of $Mg_{54}Ag_{17}$ increases the degradation rate and affects the morphology significantly

1. Introduction

Magnesium alloys are promising materials for orthopaedic applications. The advantage of magnesium is its good biocompatibility and its ability to degrade *in vivo* [1-3]. Compared to permanent implants, it can not only solve the problem of stress shielding of the bones but also can avoid the secondary removal surgery. Biodegradable materials in most clinical applications are mainly polymeric or ceramic materials, e.g., Polylactic acid (PLA) and hydroxyapatite (HA), which have inadequate mechanical strength when used for load-bearing parts [4, 5]. Compared to other biodegradable materials, magnesium alloys have higher strength and higher ductility than PLA and HA,

respectively [5]. Moreover, magnesium exhibits higher biocompatibility than PLA, since PLA has the potential to cause inflammation in the surrounding tissue [6].

In orthopedic applications, low mechanical integrity caused by local pitting prevented the application progress of magnesium alloys as biodegradable implants [7, 8]. Magnesium alloys need to exhibit suitable high strength to withstand tensile and compressive stresses during service until healing of the bone tissue [9]. Moreover, the development of biodegradable magnesium implants with good antibacterial properties is required, addressing the emergence and increase of bacteria resistant to multiple antibiotics. In earlier work improved antibacterial properties have been identified by using cast magnesium alloys with an addition of silver as the sole alloying element [10-12]. However, these works have dealt with as cast and as extruded material focused on the antibacterial effect with less emphasis on thermomechanical treatments. Relevant aspects of the microstructure, which have an impact on the mechanical properties but also the degradation behavior, are the homogeneity of the material, the grain size, the texture, and the amount and distribution of second phase particles. These aspects of the microstructure are a result of the thermomechanical treatment applied if wrought magnesium processing is used for the preparation of sheets as semifinished material, required for flat implant geometries (e.g. as bone plates). Processing of magnesium alloys is carried out at elevated temperature which includes microstructure formation mechanisms based on active deformation modes as well as recrystallization [13]. In recent years, several thermomechanical processing methods were applied on magnesium alloys to reach application specific properties [5]. Compared to other thermomechanical processing, rolling at elevated temperature has better operability of microstructure to influence mechanical properties and degradation behavior. Moreover, the rolling texture is adjustable via annealing [14].

In the present study, sheet rolling of binary Mg-Ag alloys with a silver content of up to 8 wt.% was conducted. Different rolling and annealing concepts were carried out and

assessed with respect to the microstructure development and the resulting mechanical properties as well as the degradation behavior. Several rolling and annealing temperatures were chosen. The subsequent annealing includes a typical annealing treatment for 30 min as well as a series of short time annealing steps in the range of only a few seconds for an enhanced control of the microstructure development. The relation of the rolling and annealing parameters to the microstructure is revealed, aiming to optimize the mechanical properties and degradation behavior of Mg-Ag alloys.

2. Experiments

2.1 Casting, rolling and annealing

Three alloys were used for the investigations, Q2 (Mg + 2 wt.% Ag), Q6 (Mg + 6 wt.% Ag) and Q8 (Mg + 8 wt.% Ag). They were prepared from high purity magnesium ingots (99.99 % purity; Xinxiang Jiuli Magnesium Co., Ltd., Xinxiang, China) and silver granules (99.99 % purity; ESG Edelmetall-Handel GmbH & Co. KG, Rheinstetten, Germany). The alloys were molten in a resistance furnace under protective atmosphere with sulfur hexafluoride (SF_6) and Argon (Ar) up to 750 °C and stirred for 30 min. A process based on gravity casting into rectangular crucibles was applied. The filled steel crucibles were positioned into a separate furnace to keep them at casting temperature for 15 min and to allow gas inclusions in the melt to be evaporated. Finally, the crucibles were lowered into a water bath leading to directional solidification of the melt. The chemical composition of the cast ingots analyzed by X-ray fluorescence (Bruker AXS S4 Explorer, Bruker AXS GmbH, Karlsruhe, Germany) and with a Spark Analyser (Spectrolab M, Spektro Analytical Instruments GmbH, Kleve, Germany) is collected in Table 1.

Table 1: Chemical composition of the Q2, Q6 and Q8 ingots.

Alloy	Ag wt.%	Fe wt.%	Cu wt.%	Ni wt.%	Si wt.%	Be wt.%
Q2	2.2	0.023	0.0016	<0.0002	0.0077	0.000038
Q6	6.1	0.033	0.0019	<0.0002	0.0022	0.000039

Q8	8.1	0.0017	0.0017	<0.0002	0.017	0.000037

The ingots were used to machine slaps for rolling experiments with 200 mm width, 100 mm length and a thickness of 20 mm. The solid solubility of silver in magnesium at different temperature was verified by using a phase diagram obtained via Pandat^{TM} 8.1 software (CompuTherm LLC, Middleton, USA, [15]) and its respective database (Fig. 1). At approximately 350, 400, 425 and 450 °C, the solubility of silver in magnesium is 1.4, 4.1, 6.7 and 9.9 wt.%, respectively. Solid solution annealing of the slabs was carried out at 430°C for at least 8 hours, in case of Q8 at 450 °C for 24 hours. The rolling temperature varied between 350, 400 and 450 °C. The rolling speed of the sheets was 10 m/min. The rolling schedule consisted of 13 passes with varied degree of deformation per pass $\varphi = -\ln(d_{n+1}/d_n)$, where d is the thickness of the sample and n the number of the actual pass. 4 passes with $\varphi = 0.1$ were applied followed by 9 passes with $\varphi = 0.2$. Between each two passes the samples were reheated for 15 min in an air-circulating furnace. After the final pass the rolled sheets were cooled in air. This condition is referred to as the “as-rolled condition”.

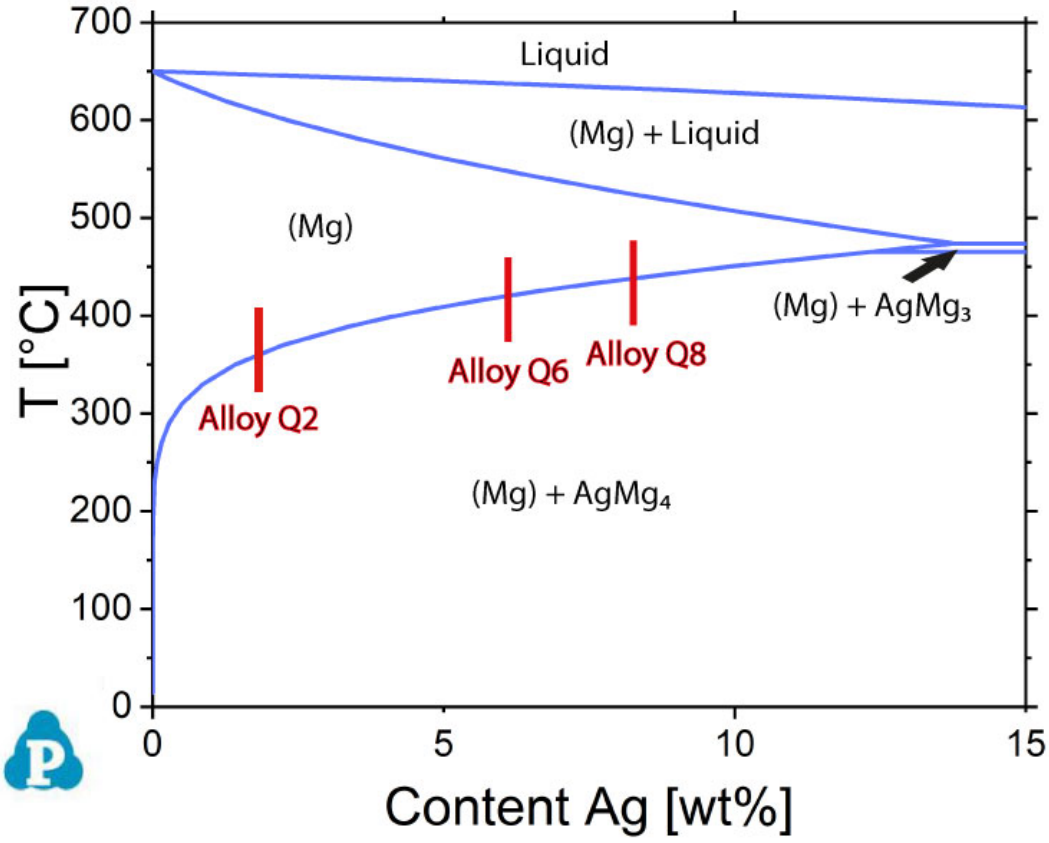

Fig. 1: Simulated partial Mg-Ag phase diagram by Pandat^{TM} 8.1 software.

A part of the as-rolled sheets was annealed. In a general annealing approach, the samples were annealed for 30 min at the respective rolling temperature. In a short time annealing approach, the as-rolled sheets were annealed at their respective rolling temperature in a resistance furnace (Vulcan A-550, Dentsply Ceramco, York, USA) for 20, 30, 40, 50 and 60 s.

2.2 Sample preparation

The samples for hardness measurement and metallographic analysis were cut from the center of the sheets. They were embedded into Demotec 30 (Demotec Metallografie, Nidderau, Germany) followed by typical grinding procedures on silicon carbon sandpapers. For metallographic and texture measurement sample surfaces were polished on rubber cloth with water-free oxide polishing suspension (OPS, Cloeren Technology GmbH, Wegberg, Germany) for at least 30 min. The samples were cleaned

with distilled water and ethanol and dried by compressed air. The samples for scanning electron microscopy (SEM) analysis were conducted with N650 planocarbon (Plano GmbH, Wetzlar, Germany) on the edge. The samples for tensile tests were cut by EDM (electrical discharging machining) along the rolling and transverse directions of the annealed sheets. The samples for immersion test were cut and ground on 1200# silicon carbon sandpapers to remove the oxides and impurities in the surface layer of the sheets.

2.3 Microstructure analysis

Light optical metallographic analysis was carried out on samples after etching in picric acid solution, which consists of water (20 mL), ethanol (100 mL), acetic acid (6.5 g), and picric acid (12-15 g; all chemicals from Sigma-Aldrich Chemie, Taufkirchen, Germany). Samples were rinsed with ethanol for several seconds and dried by compressed air. The etching time varied from 0.5 to 2 s, which depends on the silver content and state of Mg-Ag alloys. Microstructure was visualized by polarized microscopy (Leica 020-520.008 DM/LM, Leica Microsystems, Wetzlar, Germany). The grain size was measured using a linear intercept method via Olympus AnalySIS Pro software (Olympus Soft Imaging Solutions, Muenster, Germany). The distribution of precipitates in the matrix was analyzed by SEM (TESCAN vega 3 SBU, Brno, Czech Republic) in BSE (back-scattered electron) mode. The amount of precipitates was determined by ImageJ software (version 1.46r, [16]).

For phase analysis, XRD (X-ray diffraction, Bruker D8 Advance, Karlsruhe, Germany) with a Cu tube K radiation was applied. The angle (2θ) ranged from 20º to 80º. Each step the detector moved 0.01º with duration of 0.5 s. The polished surfaces of the samples were used for texture measurements on a PANalytical X'Pert Pro diffractometer setup with goniometer (XRD; Malvern Panalytical B.V., Almelo, Netherlands). Six pole figures were measured up to a tilt angle of 70° for a recalculation of the orientation distribution function and presentation of full pole figures. An open source toolbox MTEX was applied [17].

2.4 Mechanical test

The Vickers hardness (n = 5) of the annealed samples was measured on a micro-hardness tester (Emcotest Prüfmaschinen, Kuchl, Austria) in HV5 mode (test force = 49.03 N). 5 non overlapping indents were measured on each sample. Tensile tests were conducted using a universal testing machine (Zwick-Roell, Ulm, Germany) at ambient temperature and constant initial strain rate of 0.001/s. 3-5 samples were used to reveal the mechanical properties and the error margins. It is noted that the error margins are in a typical range for wrought magnesium samples.

2.5 Immersion test

The as-rolled and annealed samples were sterilized for at least 30 min in an ultrasonic bath (Sonorex RK 510S, Bandelin, Berlin, Germany) in 70 % ethanol solution. They were transferred into multi-well plates under sterile conditions and left for 30 min to evaporate the ethanol. Afterwards, cell culture medium DMEM GlutaMAX (Dulbecco's Modified Eagle's Medium, Life Technologies, Darmstadt, Germany) with 10 % FBS (Fetal Bovine Serum, PAA Laboratories, Linz, Austria) was filled in the wells. The amount of the medium was calculated according to the weight of samples (0.2 g/mL). The medium was changed after 48 and 120 hours. After 7 days, the samples were removed and rinsed with distilled water and pure ethanol. Afterwards, they were dried under vacuum for 30 min . The weight was measured before the immersion tests and after removal of the degradation products by chromic acid (180 g/L chromium (VI) oxide in distilled water). The mean degradation rates (MDR) were calculated according to [18]

$$MDR = \frac{8.76 \times 10^4 \cdot \Delta g}{A \cdot t \cdot \rho}$$

where Δg is the weight loss, A, t and ρ are total area of each sample, immersion time and density of the samples, respectively.

3. Results

3.1 Microstructure

The microstructure of the as-rolled and annealed Mg-Ag sheets is shown in Fig. 2. For the as-rolled sheets deformed microstructures with deformation bands and twins are revealed and marked by parallel lines and arrows, which still allows the grain boundaries to be distinguished. After annealing for 30 min a removal of these signs of deformation is found which is associated to the formation of a new grain structure due to static recrystallization. Interestingly, there is no visible difference in the grain size before and after annealing (Fig. 3). Thus, a steady state of the microstructure development during rolling and annealing has been achieved.

The sheets rolled at the lowest rolling temperature of 350 °C also have the smallest grain sizes for alloys Q2 and Q6. However, the average grain size of Q6 is smaller than that of Q2 at this temperature (Fig. 3). Furthermore, Q6 shows an inhomogeneous grain structure of a bi-modal type with sections of smaller and larger grains, respectively.

With increasing temperature the average grain size increases. After rolling and annealing at 400 °C, Q2 and Q6 obtained a homogeneous grain structure (Fig. 2). In this case also the higher content of Ag in Q6 leads to the formation of larger grains compared to Q2 (Fig. 3). Rolling at 450 °C increases these effects, i.e. grains grow larger in general and Q6 shows even larger grains compared to Q2. At this temperature also results for Q8 alloy were obtained, revealing a slightly coarser grained structure compared to Q6. There was abnormal growth of grains in Q2 at 450 °C.

Micrographs taken by scanning electron microscopy were used to analyze the appearance and morphology of precipitates. No precipitates are observed in Q2 at any rolling temperature. Contrary, many precipitates exist in the Q6 sheets rolled and annealed at 350 or 400 °C (Fig. 4, upper panel). Obviously, such precipitates formed during the rolling procedure. They are concentrated in bands or stringers parallel to the rolling direction. The areas with precipitation are rich in silver, determined by EDS (Fig.

4, lower panel). The area fraction of precipitates in Q6 is displayed in Fig. 5a. At higher rolling temperature of 400 °C, their content decreased distinctly. In case of alloy Q8, rolled at 450 °C, also no precipitates are found. According to XRD patterns, the precipitates existing in Q6 are consistent with $Mg_{54}Ag_{17}$ (Fig. 5b, [19]).

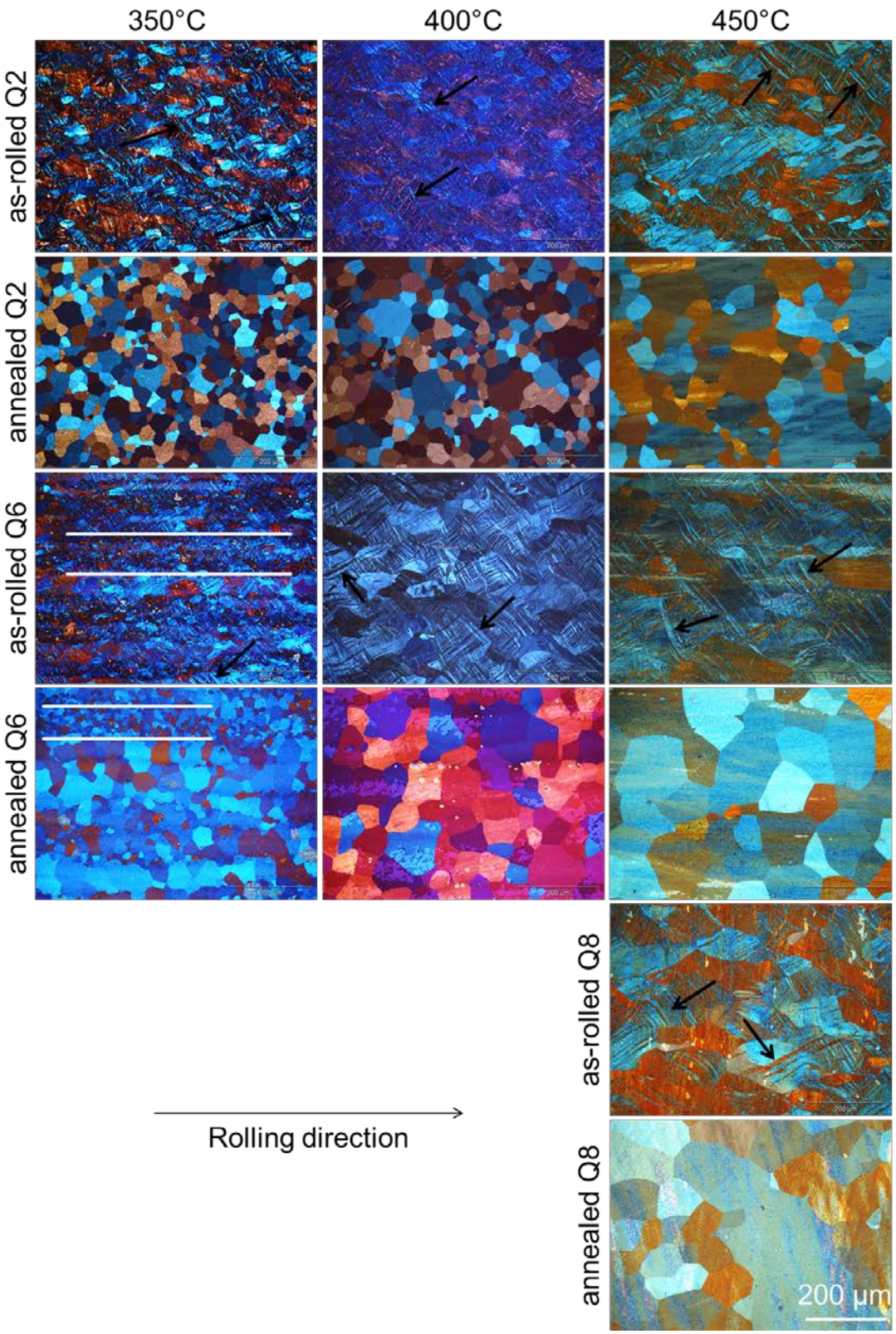

Fig. 2: Microstructures (normal plane) of as-rolled and annealed Q2, Q6 and Q8 alloys at different temperatures.

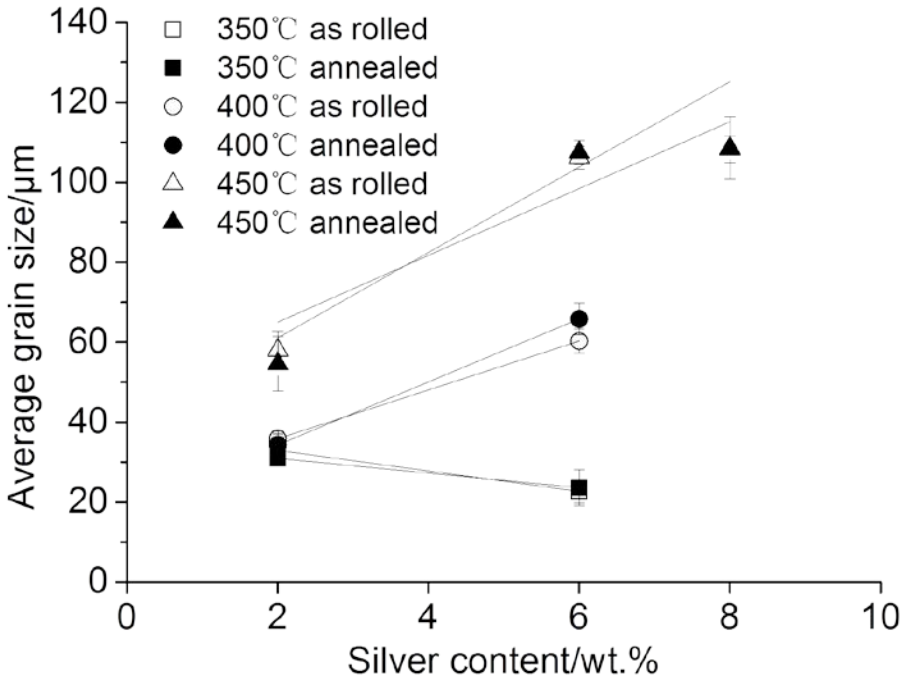

Fig. 3: Average grain size development during sheet rolling and annealing at various temperatures as a function of the Ag-content (lines are to guide the eyes).

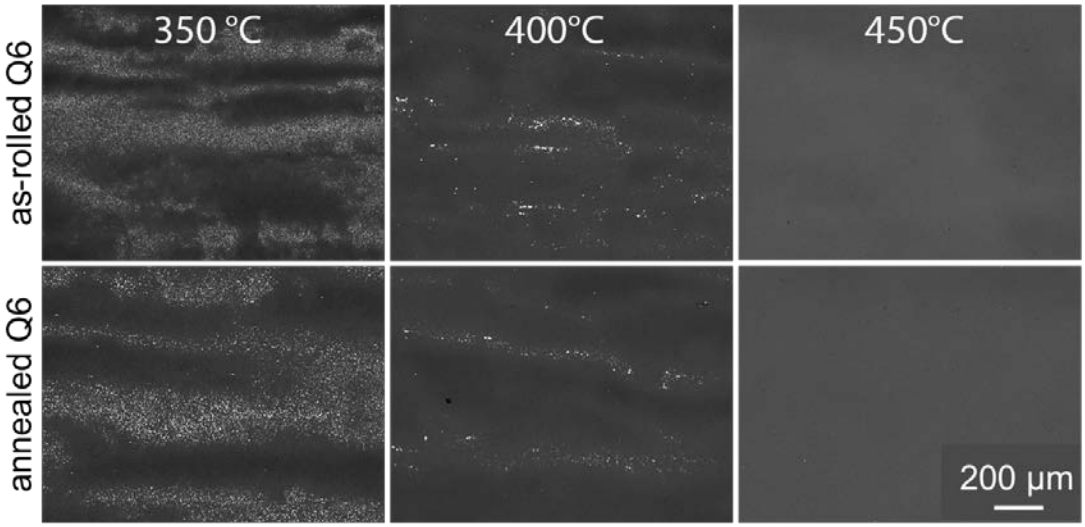

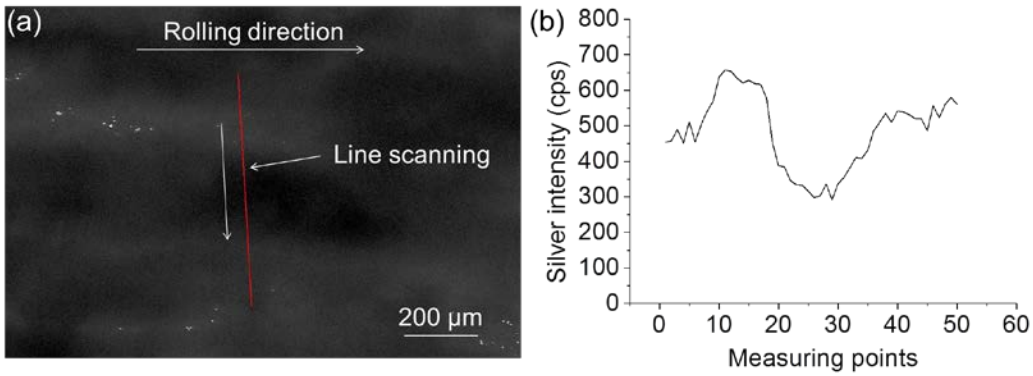

Fig. 4: SEM images (BSE, back-scattered mode) of precipitate distribution along rolling direction of the Q6 alloy (upper panel) and EDS analysis of relative silver concentration in Q6 annealed at 400°C (lower panel). The red line in (a) is the scanning trace and the curve in (b) displays the silver intensity at different measuring points along the red line. No precipitates were observed in Q2 and Q8 alloys.

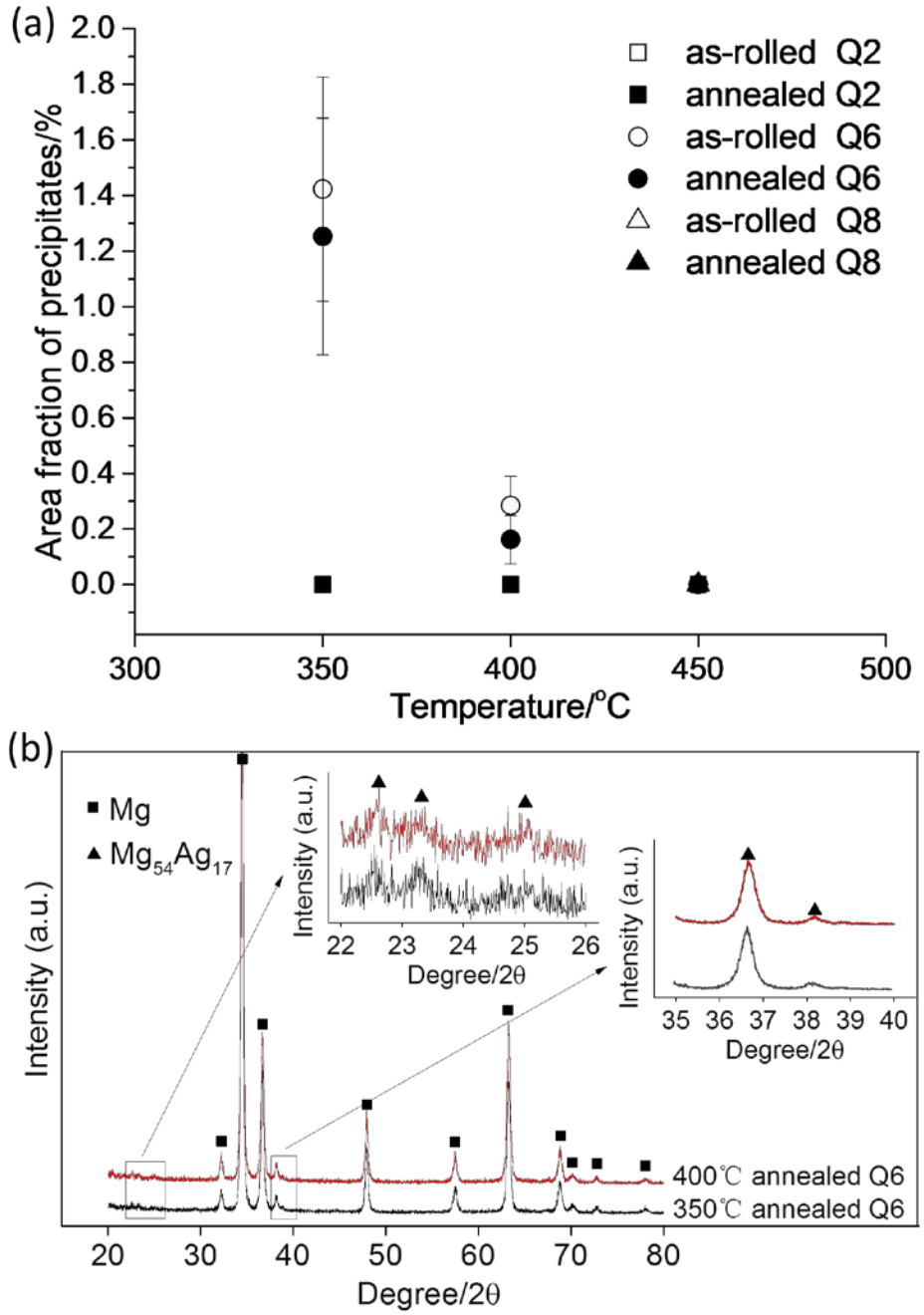

Fig. 5: Area fraction of precipitates in Q2, Q6 and Q8 (a) and X-ray diffraction of Q6 (b).

3.2 Texture evolution

In Fig. 6, the textures of the sheets are collected by showing their (0001) basal plane and (10-10) prismatic plane pole figures. In all cases, i.e. the three alloys at the different rolling temperatures before and after annealing, there is a similar development of a

basal texture which orients the majority of grains with their basal planes parallel to the sheet plane. Concurrent to this, prismatic planes are randomly distributed parallel to the normal direction of the sheet. Furthermore, the angular spread of basal planes is broader towards the rolling direction compared to the transverse direction which leads to very typical textures of classical magnesium sheets [20]. Differences in the texture can be described by the intensity of the pole figures, mainly varied in its significance of the basal plane alignment. The as-rolled conditions, however, do not exhibit a clear tendency. During annealing a slight weakening of the texture can be visualized at the lowest temperature of 350 °C. At higher temperatures the tendency to texture strengthening becomes obvious. This finding corresponds directly to the tendency of grain growth during annealing.

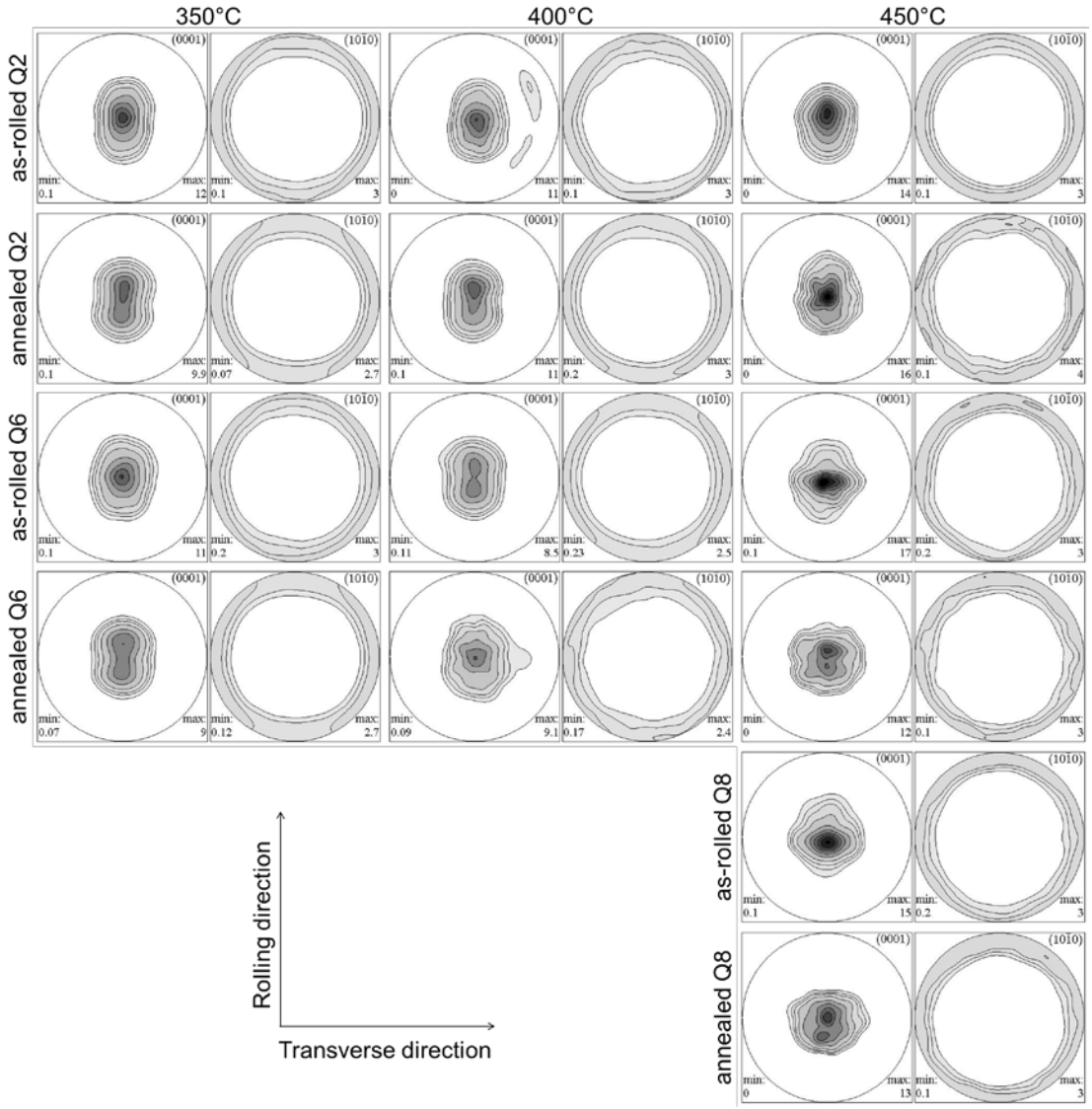

Fig. 6: Texture evolution of Q2, Q6 and Q8 alloys with temperature after rolling and annealing.

3.3 Vickers hardness and mechanical properties

The as-rolled sheets exhibit a higher hardness than the annealed counterparts because of their work hardened condition after the final rolling pass (Fig. 7). Moreover, the hardness of the annealed sheets drops with increasing temperature. In both conditions, the hardness increased gradually with increasing silver content. This finding also corresponds to the above described grain coarsening as well as texture strengthening.

The mechanical properties of the sheets in the annealed condition (30 min. annealing) are displayed in Table 2. Generally, all sheets reveal higher yield strength along the

transverse direction than along the rolling direction. However, the samples, especially Q2, have higher fracture strain along the rolling direction. Silver addition leads to an increase of yield stress and ultimate strength in both directions. The increase of rolling temperature results in a drop of tensile strength and fracture strain of annealed Q2 along the rolling and transverse direction and annealed Q6 along the rolling direction.

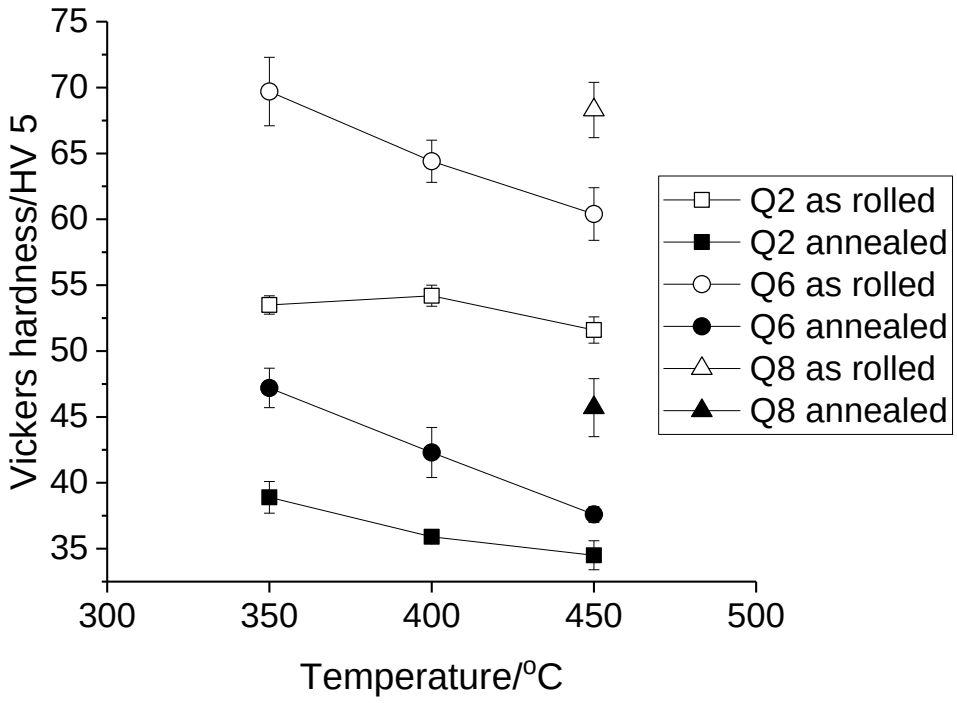

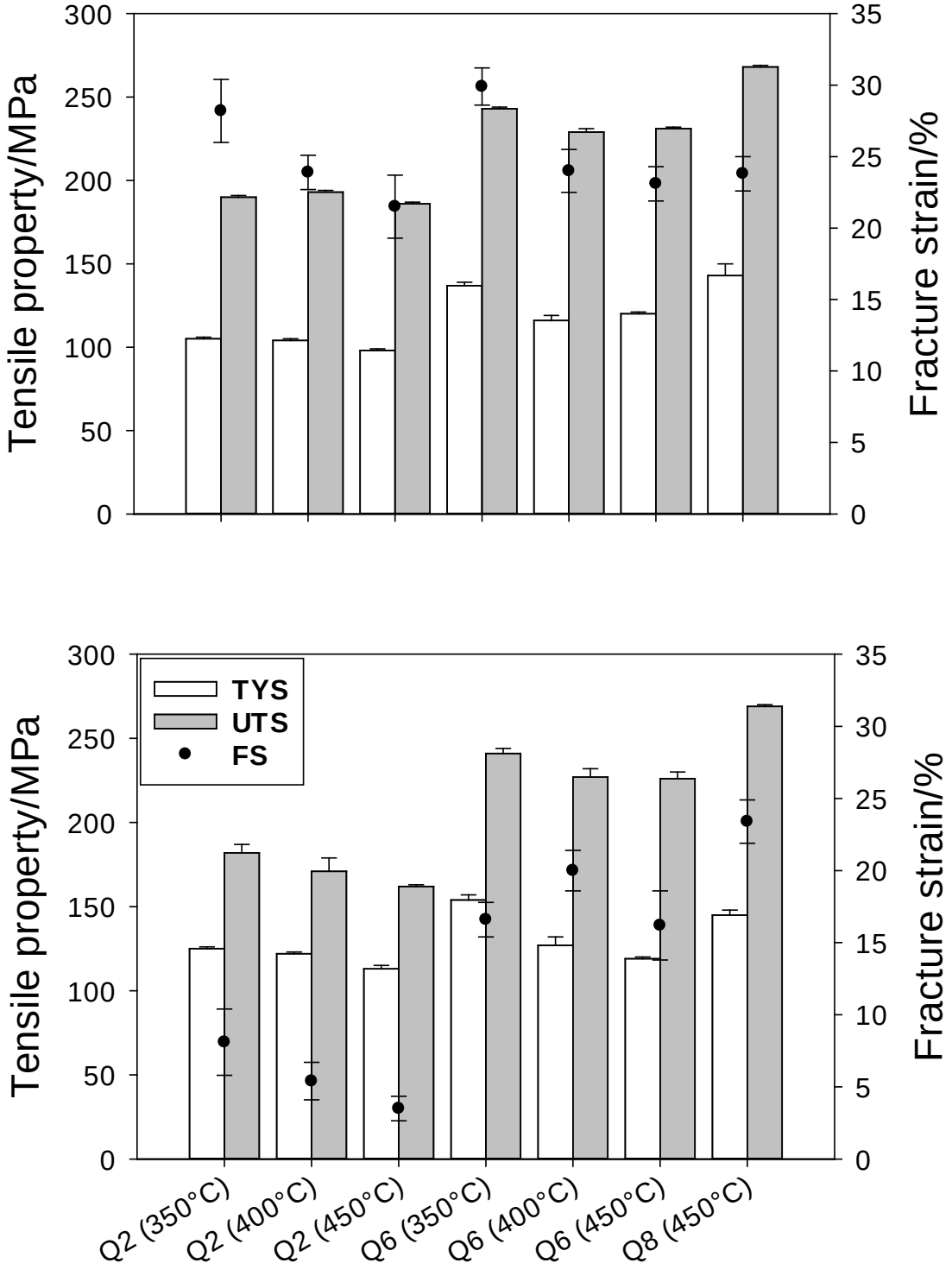

Fig. 7: Mechanical properties: Upper panel: Hardness variation of the alloys. The lines show the trend with increasing temperature. Middle: Tensile properties (tensile yield strength – TYS; ultimate tensile strength – UTS, Fracture strain – FS) in rolling direction. Lower panel: Properties in transverse direction.

3.4 Mean degradation rate and degradation morphology

In Fig. 8, Q6 rolled at 350 °C possesses the highest mean degradation rate followed by Q6 rolled at 400°C and Q2 rolled at 350 °C. There is no significant difference between the degradation rates of as-rolled and annealed alloys, except for Q2 rolled at 350 °C. A slight drop of the mean degradation rate was observed in the as-rolled Q2 alloy after general annealing at 350 °C for 30 min. Hence, general annealing of Q2 has an effect at this temperature. This may be linked to some remaining precipitates or silver in the as-rolled state. At higher temperatures, the drop of the degradation rate is not visible. With increasing temperature the mean degradation rate of Q6 declined gradually. This is consistent with an increased degradation rate due to precipitates (for comparison see the area fraction of precipitates in Fig. 3, which follows exactly the same trend) whereas silver in solid solution does not affect it. At 450 °C, Q2, Q6 and Q8 had very low degradation rate. Their mean degradation rates were comparable.

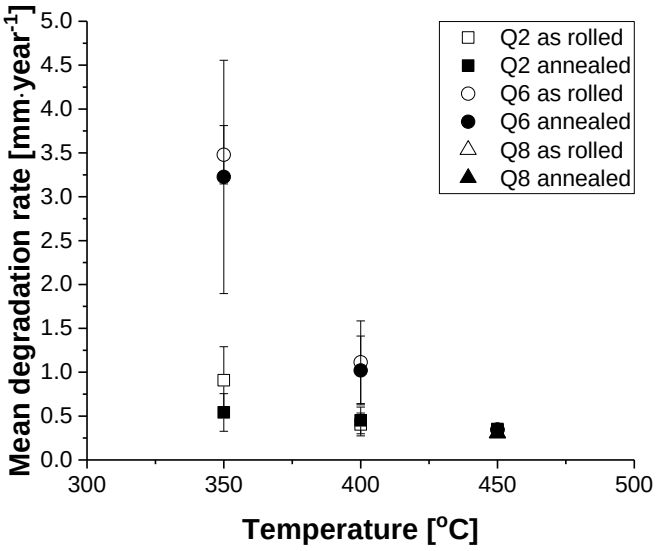

Fig. 8: The mean degradation rates of as-rolled and annealed Q2, Q6 and Q8 alloys.

The morphology of the alloys after removal of degradation products is shown in Fig.9. In Q2 rolled at 350 °C, some big and deep pits exist on the surface. In Q2 rolled at 400 °C, there are many small pits on the surface. However, in Q2 rolled at 450 °C, small

platforms instead of pits are revealed. Hence, higher rolling temperature relieved pitting effectively. The morphology changes of annealed Q6 show the same trend with increasing temperature. In rolled sheets at 350 °C, the surface of annealed Q6 has very severe local pitting. When the temperature is increased to 400 °C, many pits distribute along the rolling direction of Q6, which are indicated by the parallel lines in Fig. 9. At 400 and 450 °C, the contour of grains and twins can be observed on the surface of as-rolled Q6 and Q8 (indicated by white arrows), which is associated with intergranular degradation. It is assumed that many very fine precipitates distribute towards twins and grain boundaries during rolling of Q6 (Fig. 9). After annealing only few small precipitates exist at the grain boundaries of Q6. Thus, the micro-galvanic degradation occurred with the interior of grains acting as the anode. As a result, those samples (as-rolled Q6 and Q8) exhibit a rougher surface than the annealed alloys, even though the degradation rates of as-rolled and annealed alloys are similar. In contrast, the surfaces of the annealed Q6 and Q8 rolled at 450°C show a homogeneous morphology without pits.

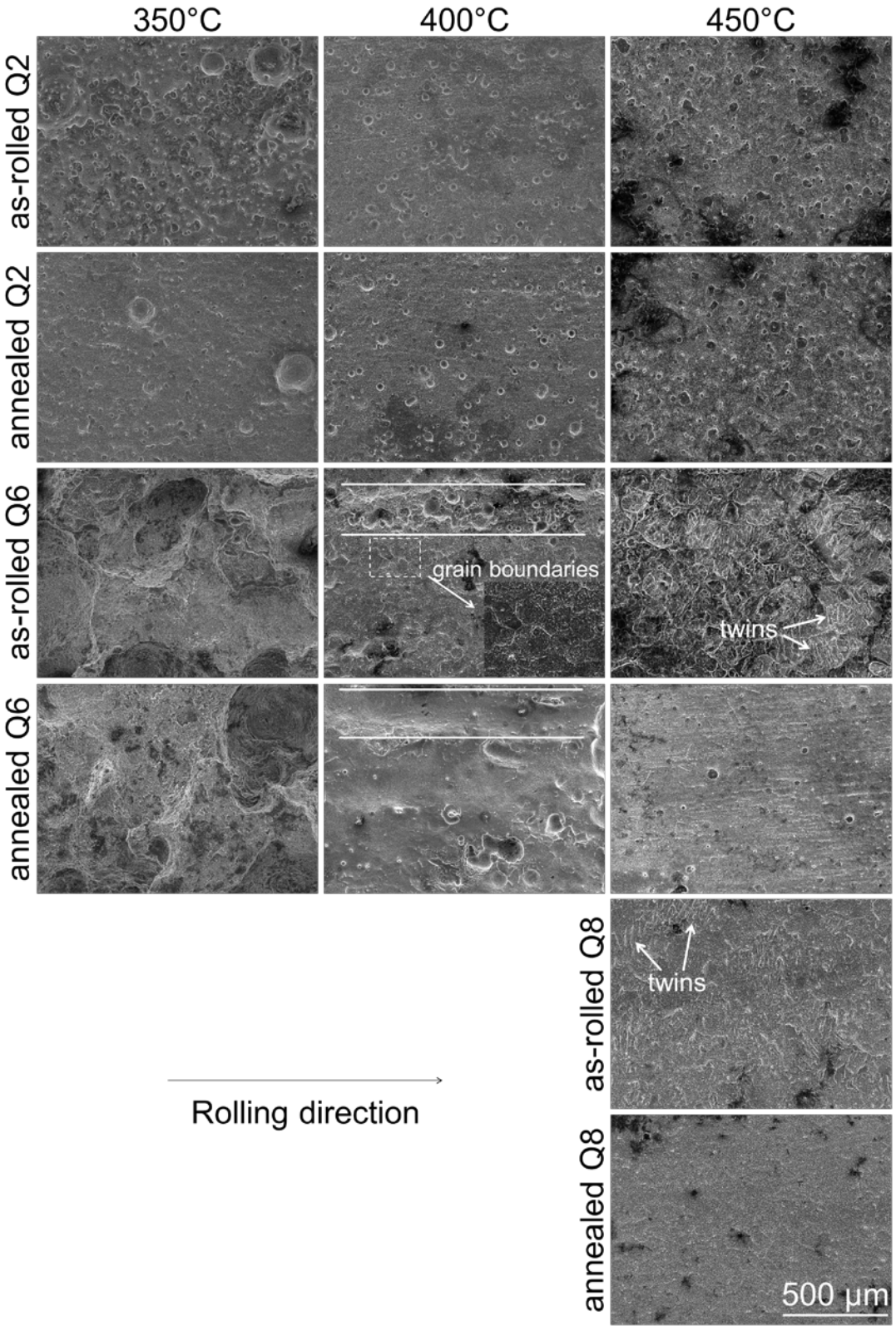
350°C
400°C
450°C
as-rolled Q2
annealed Q2
as-rolled Q6
annealed Q6
as-rolled Q8
annealed Q8
grain boundaries
twins
twins
Rolling direction
500 µm

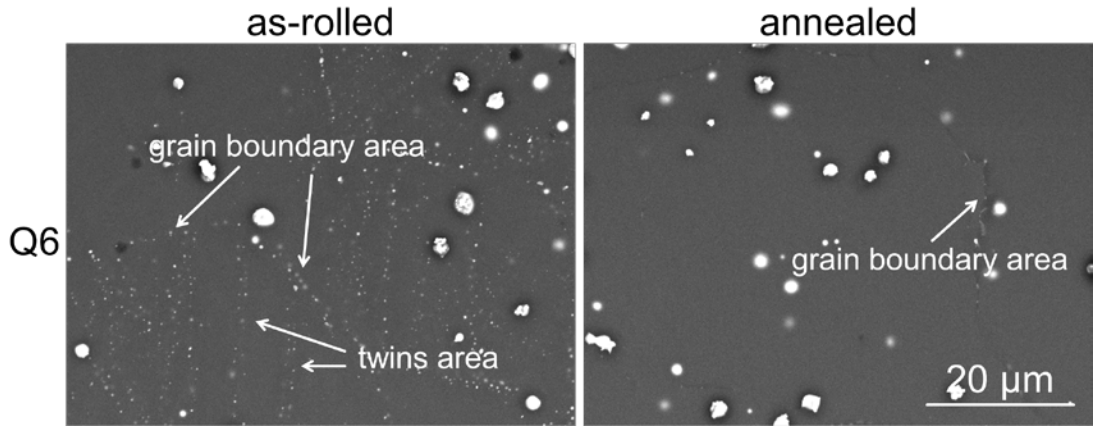

Fig. 9: Morphologies of Q2, Q6 and Q8 alloys in SE (secondary electron) mode (up), and more detailed precipitate distribution in as-rolled and annealed Q6 at 400°C in BSE (back-scattered electron) mode (below).

3.5 Short time annealing and changes of grain size

To avoid distinct grain growth during annealing and to control the grain structure development, short time annealing in the range below 60 s was carried out for tailoring the material properties. The microstructure development is shown in Fig. 11.

Annealing at 350 °C starts to reduce the bimodal character, i.e. a grain structure consisting of a fraction of smaller grains embedded into a fraction with larger grains, of the microstructure if compared to the microstructure in the as-rolled condition in Fig. 1. This microstructure appears more homogeneous after 60s annealing. Annealing at 400 °C immediately leads to fully recrystallized microstructures after 30 s followed by grain growth. Although the microstructure of Q6 annealed at 450 °C for 20 s is complex, the tendency to recrystallization and grain growth appears to be enhanced at this high temperature. For alloy Q8 with the highest amount of Ag not much change is found during the short time annealing and an inhomogeneous partly recrystallized microstructure persists. It is worthwhile to repeat that this material is fully recrystallized along with the coarsest grain structure of this study after 30 min annealing (Figs. 2 and 3).

Fig. 11 displays the average grain size development during short time annealing. A distinct drop in the beginning is associated with the onset of recrystallization and the formation of small recrystallized grains. In tendency, there seems to be a delay in grain growth at these short annealing times with increasing Ag content which is contrary to the finding after 30 min annealing including grain growth.

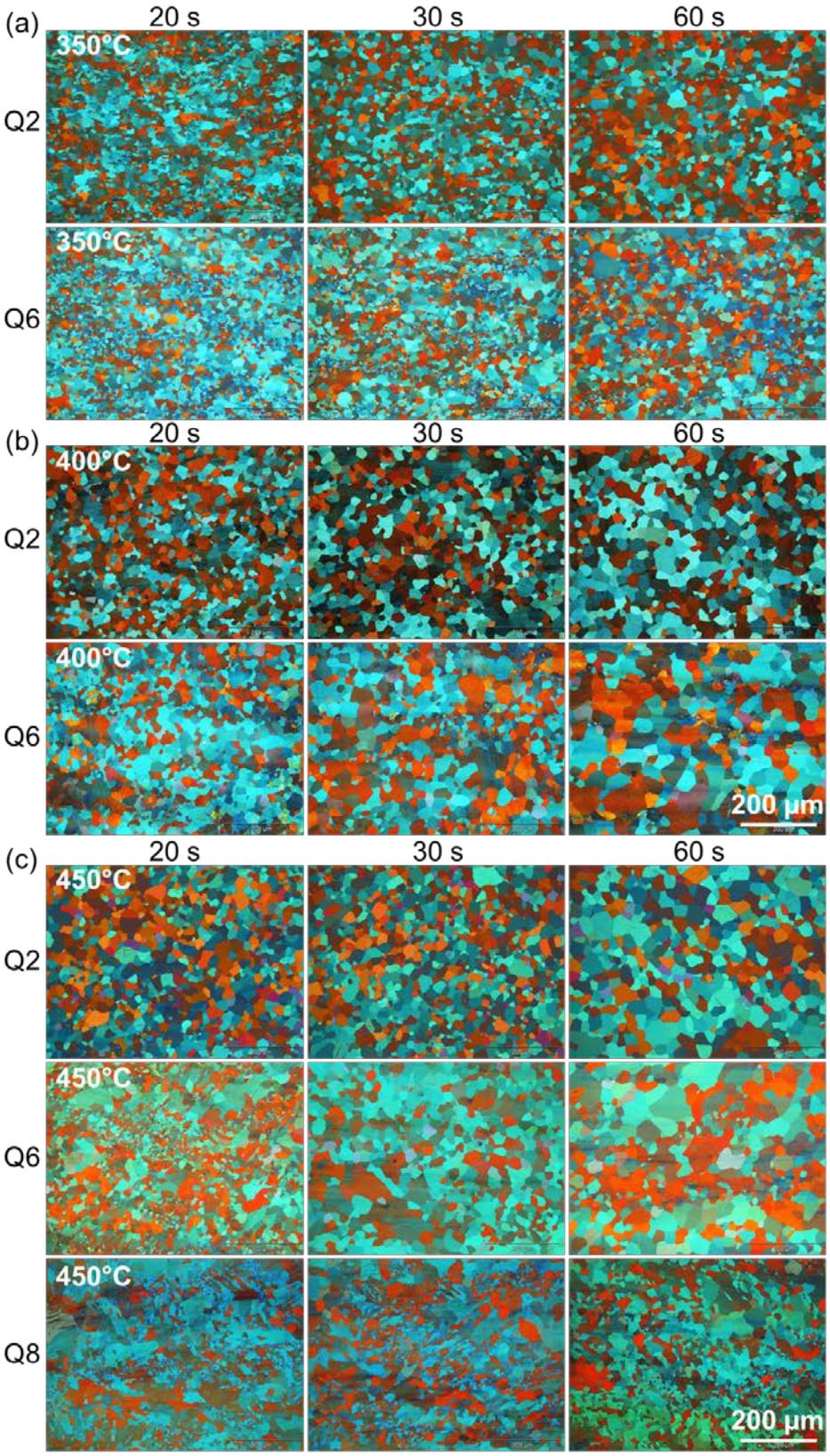

Fig. 10: Microstructure of the as-rolled alloys after short time annealing at different temperatures: a) 350 °C, b) 400 °C, c) 450 °C.

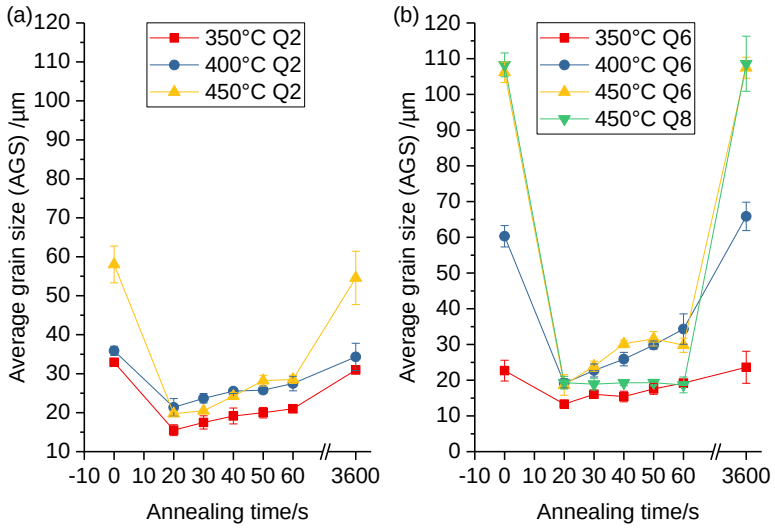

Fig. 11: Grain size development during short time annealing at various temperatures (rolling temperature and annealing temperature are always equal); a) Q2, b) Q6, c) Q8

3.6 Mechanical properties after short time annealing

In Fig. 12, the as-rolled Mg-Ag alloys exhibit the highest hardness which drops with the annealing time gradually. Again, higher hardness is maintained with higher Ag-content. Interestingly, no distinct change with the annealing temperature is found.

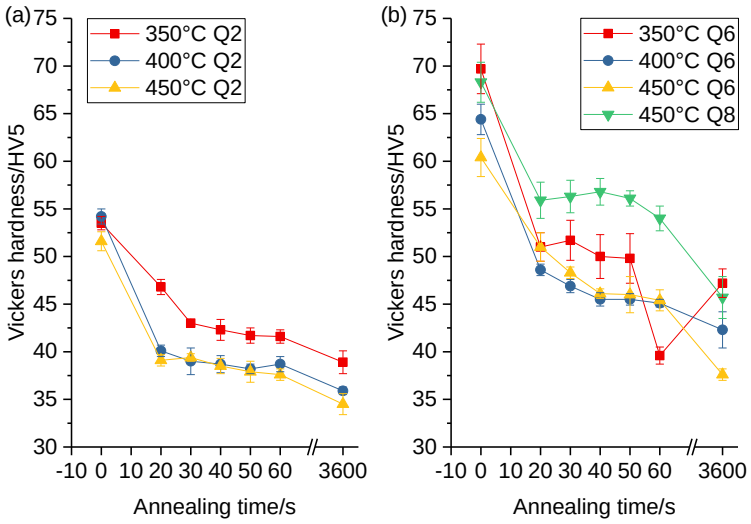

Fig. 12: Hardness changes with annealing time and temperature.

In Fig. 13 the resulting mechanical properties of the sheets annealed for only 30 s are collected which allows comparison to those after 30 min annealing. The short time

annealed sheets maintained higher tensile strength compared to the general annealed alloys. Also the yield strength shows a substantial increase compared to that of the alloys after annealing for 30 min at the expense of a moderate reduction of the fracture strain. Again, Q2 has very low fracture strain along the transverse direction. The Q6 rolled at 350 °C has a substantial drop of fracture strain when compared with the one annealed for 30 min. Via short time annealing, the Q6 rolled at 400 and 450 °C as well as Q8 rolled at 450 °C obtained good fracture strain along rolling and transverse direction.

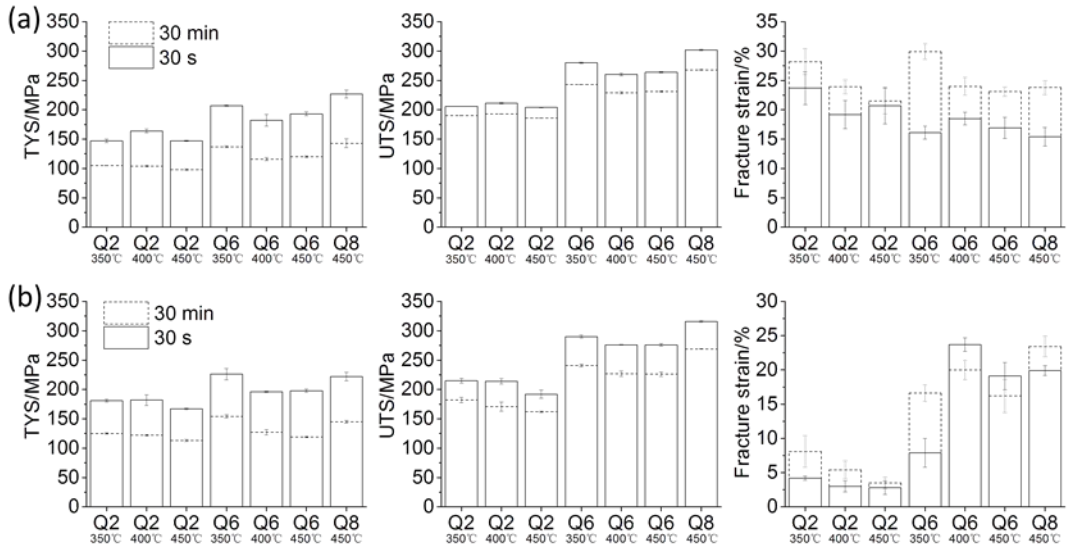

Fig. 13: Comparison of mechanical properties along rolling (a) and transverse direction after annealing for 30 s and 30 min.

4. Discussion

4.1 Microstructure development during processing

Static recrystallization is driven by the stored energy after thermo-mechanical treatment (rolling) [21-23]. The grain size development of the Mg-Ag sheets is directly dependent on the rolling temperature or the annealing temperature, respectively. Also the tendency to form or maintain precipitates increases with increasing Ag-content. The solvus of

silver in magnesium at 350 °C is around 1.4 wt.% according to the respective database of PandatTM 8.1 software. Still, Q2 rolled at 350°C showed little precipitation. At 400 °C, the solvus of silver was lower than 6 wt.% in magnesium [24]. Thus, at lower rolling temperatures and higher Ag-content more precipitates are revealed with specific impact on the microstructure and its development. If stringers of precipitates occur parallel to the rolling direction, very small grains are found in the vicinity of these particles. This results in an inhomogeneous microstructure potentially of a bimodal type. It also confirms a growth limitation effect for the grains close to such particles. In case of rolling (and annealing) at 350 °C there is a decrease of the average grain size if the Ag content is increased from 2 wt.% to 6 wt.% which is directly associated with the higher tendency to form precipitates. However, for rolling at 400 °C an increase of the average grain size is revealed and at 450 °C this increase is very significant. At this high temperature a further increase of the Ag-content to 8 wt.% does not lead to significant changes concurrent to the increase of potential precipitations. It should be noted that rolling procedures cannot be exactly maintained at the scheduled temperatures but the resulting temperatures will be somewhat lower.

In comparison to classically rolled sheets the resulting microstructures are very coarse grained [25], even if the rolling temperatures are low. In general, the grain size of metallic materials is always enlarged with the increase of the annealing temperature and time until equilibrium [26, 27]. Abnormal grain growth can even take place in magnesium alloys [26], when annealing temperatures near the melting point are applied [28, 29]. If Ag is in solid solution it is hypothesized that static recrystallization is even accelerated compared to conventional Mg-Al alloys. Considering the fast recrystallization rate of as-rolled Mg-Ag alloys, short time annealing is used as a suitable approach for grain refinement. In this case it is more obvious that grain nucleation and nucleus growth during static recrystallization is somewhat retarded with increasing Ag-content. In Fig. 11 an increase of the grain nucleation rate is indirectly visible due to increasing drop of the average grain size after the start of the annealing

with increasing temperature. However, increasing Ag-content increases the formation of inhomogeneous, i.e. partly recrystallized, microstructures hinting towards a delay in grain growth. The latter may be associated with the appearance of precipitates. Although the short time annealing is not appropriate for industrial applications requiring huge amounts of material, it may be a suitable concept to produce and tailor material for implant applications.

4.2 Impact on the mechanical properties

Ag in solid solution and precipitates influence not only on the microstructure development but also to the mechanical properties. With an increase of the temperature, grains enlarged and precipitates dissolved, so the hardness dropped gradually. At 450°C, no precipitates in Q6 and Q8 could be observed, since the processing temperature is higher than the solid solution temperature of 8 wt.% silver in magnesium according to the respective database of Pandat^{TM} 8.1 software. The hardness of Q2, Q6 and Q8 at 450°C increased gradually because of the increment of silver solubility in magnesium. The hardness of annealed Mg-Ag sheets is a combined effect of fine grains, precipitates and solution strengthening on the hardness (see Fig. 3, 4a and 6).

The grain size in Mg-Ag alloys also influenced the mechanical strength. Annealing for 30 min eliminated all twins in Mg-Ag alloys, but the grains are very large. As a result, the general annealing deteriorated the final mechanical strength of Mg-Ag alloys. On the other hand, the annealing procedure was operated to control the mechanical properties [24-26], i.e short time annealing. In tensile tests, fine-grained magnesium is stronger than coarse grained samples due to a typical grain boundary impedence of dislocation motion. Furthermore, the strength of Mg-Ag alloys is also influenced by the silver solubility, so higher silver content leads to higher yield and ultimate strength. Moreover, in tensile tests along rolling and transverse directions, the deformation behavior is anisotropic which is correlated with the rolling texture [30]. The angular spread of basal planes is broader towards the rolling direction compared to the

transverse direction. The tensile properties are different in these two directions. Hence, the grain size, silver amount and texture define the tensile properties.

4.3 Impact on the degradation behavior

The precipitates in Mg-Ag alloys have a grain refining effect but accelerate degradation rate and induce pitting. The degradation shows a complex behavior mainly consistent with the precipitation (see Fig. 4 and 7). The SEM pictures exhibit pitting most likely consistent with the respective precipitates (see Fig. 3 and Fig. 10). Both the amount and position of precipitates have significant influence on the degradation of Mg-Ag alloys. More precipitates can induce higher degradation rate which is adverse to the further mechanical integrity during the degradation [7, 8, 31]. A recent study has identified a novel Mg7Ag3 intermetallic phase, which could also be formed during thermomechanical treatment [32], and could be interesting to deeply study the influence of different intermetallics on degradation. However, here the aim was to optimize the material to low or no precipitations. Although twins exist in these as-rolled alloys, they have no visible influence on the degradation rate of Mg-Ag alloys. Instead, the precipitates at grain boundaries and twins evoked a rough morphology. Since pitting and rough surface can induce fast loss of mechanical integrity at early stage of implantation [7, 8], it is necessary to obtain low degradation rate and eliminate pitting. This could be reached by adjusting the rolling and annealing temperature, which inhibited precipitation even in the Q8 alloy. The silver distribution became more homogeneous which is supposed to be beneficial for the degradation behavior. As a result, the degradation rate dropped down along with the elevated temperature and became stable and the degradation surface became homogeneous. Thus, the Mg-Ag alloy with low silver-content can be processed at relative low temperature to obtain fine-grained microstructure without precipitates. If a higher amount of silver should be alloyed into magnesium, it is necessary to use a high enough rolling temperature to avoid the precipitates followed by short time annealing.

5. Conclusion

Rolling of Mg-Ag-alloys to sheets leads to microstructures revealing enhanced grain growth with increasing Ag content as a result of static recrystallization. This finding is evident if Ag is maintained in solid solution whereas the formation of precipitates leads to grain refinement, i.e. retarded grain growth during recrystallization. Short time annealing allows to distinguish between grain nucleation being delayed during static recrystallization whereas grain growth is enhanced with increasing Ag content. Ag increases the mechanical strength of alloys. Short time annealing has been proven to allow a distinct microstructure design for increasing strength properties and maintain ductility. Higher Ag content also requires higher temperatures during processing to dissolve precipitates, thus slow down the high degradation rate and relieve pitting. Precipitates of $Mg_{54}Ag_{17}$-type have been proven to seriously increase degradation rate.

Acknowledgement

The author Zhidan Liu thanks for the financial support from China Scholarship Council (CSC). The authors would like to thank Alexander Reichart for technical assistance in the rolling procedure, Gert Wiese in the metallographic preparation and Björn Wiese in the simulation of Mg-Ag phase diagram. This work was supported by the Helmholtz Virtual Institute “In vivo studies of biodegradable magnesium-based implant materials (MetBioMat)” [grant number VH-VI-523].

Declarations of interest: None

References

[1] P. Zartner, R. Cesnjevar, H. Singer, M. Weyand, First successful implantation of a biodegradable metal stent into the left pulmonary artery of a preterm baby, Catheterization and Cardiovascular Interventions, 66 (2005) 590-594.

[2] F. Witte, J. Fischer, J. Nellesen, H.-A. Crostack, V. Kaese, A. Pisch, F. Beckmann, H. Windhagen, In vitro and in vivo corrosion measurements of magnesium alloys, Biomaterials, 27 (2006) 1013-1018.

[3] F. Witte, V. Kaese, H. Haferkamp, E. Switzer, A. Meyer-Lindenberg, C. Wirth, H. Windhagen, In vivo

corrosion of four magnesium alloys and the associated bone response, Biomaterials, 26 (2005) 3557-3563.
[4] M.P. Staiger, A.M. Pietak, J. Huadmai, G. Dias, Magnesium and its alloys as orthopedic biomaterials: a review, Biomaterials, 27 (2006) 1728-1734.
[5] X.-N. Gu, Y.-F. Zheng, A review on magnesium alloys as biodegradable materials, Frontiers of Materials Science in China, 4 (2010) 111-115.
[6] K.A. Athanasiou, C.M. Agrawal, F.A. Barber, S.S. Burkhart, Orthopaedic applications for PLA-PGA biodegradable polymers, Arthroscopy: The Journal of Arthroscopic & Related Surgery, 14 (1998) 726-737.
[7] S. Zhang, X. Zhang, C. Zhao, J. Li, Y. Song, C. Xie, H. Tao, Y. Zhang, Y. He, Y. Jiang, Research on an Mg–Zn alloy as a degradable biomaterial, Acta Biomaterialia, 6 (2010) 626-640.
[8] X. Gu, W. Zhou, Y. Zheng, Y. Liu, Y. Li, Degradation and cytotoxicity of lotus-type porous pure magnesium as potential tissue engineering scaffold material, Materials Letters, 64 (2010) 1871-1874.
[9] M.B. Kannan, R.S. Raman, In vitro degradation and mechanical integrity of calcium-containing magnesium alloys in modified-simulated body fluid, Biomaterials, 29 (2008) 2306-2314.
[10] Z. Liu, R. Schade, B. Luthringer, N. Hort, H. Rothe, S. Mueller, K. Liefeith, R. Willumeit-Roemer, F. Feyerabend, Influence of the Microstructure and Silver Content on Degradation, Cytocompatibility, and Antibacterial Properties of Magnesium-Silver Alloys In Vitro, Oxidative Medicine and Cellular Longevity, 2017 (2017) 14.
[11] D. Tie, F. Feyerabend, N. Hort, D. Hoeche, K.U. Kainer, R. Willumeit, W.D. Mueller, In vitro mechanical and corrosion properties of biodegradable Mg–Ag alloys, Materials and Corrosion, 65 (2014) 569-576.
[12] D. Tie, F. Feyerabend, W.-D. Müller, R. Schade, K. Liefeith, K.U. Kainer, R. Willumeit, Antibacterial biodegradable Mg-Ag alloys, European Cells and Materials, 25 (2013) 284-298.
[13] C. Bettles, M. Barnett, Advances in wrought magnesium alloys: Fundamentals of processing, properties and applications, Elsevier, 2012.
[14] J. Bohlen, J. Wendt, M. Nienaber, K.U. Kainer, L. Stutz, D. Letzig, Calcium and zirconium as texture modifiers during rolling and annealing of magnesium–zinc alloys, Materials Characterization, 101 (2015) 144-152.
[15] Computherm, Pandat ™, in, http://www.computherm.com/, 2018.
[16] C.A. Schneider, W.S. Rasband, K.W. Eliceiri, NIH Image to ImageJ: 25 years of image analysis, Nat Meth, 9 (2012) 671-675.
[17] F. Bachmann, R. Hielscher, H. Schaeben, Texture analysis with MTEX–free and open source software toolbox, in: Solid State Phenomena, Trans Tech Publ, 2010, pp. 63-68.
[18] F. Feyerabend, M. Johannisson, Z. Liu, R. Willumeit-Römer, Influence of various sterilization methods on hardness, grain size and corrosion rate of a Mg6Ag-alloy, BioNanoMaterials, 16 (2015) 51-58.
[19] G. Kreiner, S. Spiekermann, Crystal Structure of ϵ-Ag7+xMg26–x – A Binary Alloy Phase of the Mackay Cluster Type, Zeitschrift für anorganische und allgemeine Chemie, 627 (2001) 2460-2468.
[20] Z. Zeng, Y. Zhu, S. Xu, M. Bian, C. Davies, N. Birbilis, J. Nie, Texture evolution during static recrystallization of cold-rolled magnesium alloys, Acta Materialia, 105 (2016) 479-494.
[21] A. Rollett, F. Humphreys, G.S. Rohrer, M. Hatherly, Recrystallization and related annealing phenomena, Elsevier, 2004.

[22] R. Doherty, D. Hughes, F. Humphreys, J. Jonas, D.J. Jensen, M. Kassner, W. King, T. McNelley, H. McQueen, A. Rollett, Current issues in recrystallization: a review, Materials Science and Engineering: A, 238 (1997) 219-274.
[23] C. Su, L. Lu, M. Lai, Recrystallization and grain growth of deformed magnesium alloy, Philosophical Magazine, 88 (2008) 181-200.
[24] A. Nayeb-Hashemi, J. Clark, The Ag-Mg (silver-magnesium) system, Bulletin of Alloy phase diagrams, 5 (1984) 348-358.
[25] J. Bohlen, M.R. Nürnberg, J.W. Senn, D. Letzig, S.R. Agnew, The texture and anisotropy of magnesium–zinc–rare earth alloy sheets, Acta Materialia, 55 (2007) 2101-2112.
[26] A. Yamamoto, M. Kakishiro, M. Ikeda, H. Tsubakino, Grain refinement on AZ31 magnesium alloy by highly strained and annealed method, in: Materials science forum, Trans Tech Publ, 2004, pp. 669-672.
[27] Y. Huang, L. Froyen, Recovery, recrystallization and grain growth in Fe 3 Al-based alloys, Intermetallics, 10 (2002) 473-484.
[28] M. Perez-Prado, O. Ruano, Texture evolution during annealing of magnesium AZ31 alloy, Scripta materialia, 46 (2002) 149-155.
[29] G. Higgins, Secondary recrystallisation in magnox AL 80, Journal of Nuclear Materials, 8 (1963) 153-159.
[30] Y. Prasad, K. Rao, Processing maps for hot deformation of rolled AZ31 magnesium alloy plate: Anisotropy of hot workability, Materials Science and Engineering: A, 487 (2008) 316-327.
[31] Y. Sun, B. Zhang, Y. Wang, L. Geng, X. Jiao, Preparation and characterization of a new biomedical Mg–Zn–Ca alloy, Materials & Design, 34 (2012) 58-64.
[32] Y. Ren, H. Zhao, L. Wang, B. Yang, H. Li, S. Sun, H. Pan, G. Qin, Evidence of a novel intermetallic Mg7Ag3 phase in Mg-Ag binary alloy system, Journal of Applied Crystallography, 51 (2018) 844-848.